

# Investigation of radiation absorption and X-ray fluorescence properties of medical imaging scintillators by Monte Carlo methods

D. Nikolopoulos<sup>a</sup>, I. Kandarakis<sup>a,\*</sup>, D. Cavouras<sup>a</sup>, I. Valais<sup>a</sup>, D. Linardatos<sup>a</sup>, C. Michail<sup>a</sup>, S. David<sup>a</sup>, A. Gaitanis<sup>a</sup>, C. Nomicos<sup>b</sup>, A. Louizi<sup>c</sup>

<sup>a</sup>Department of Medical Instruments Technology, Technological Educational Institution of Athens, Agiou Spiridonos, Aigaleo 12210, Athens, Greece

<sup>b</sup>Department of Electronics, Technological Educational Institution of Athens, Agiou Spiridonos, Aigaleo 12210, Athens, Greece

<sup>c</sup>Medical Physics Department, Athens University, Medical School, 75 Mikras Asias str. 11527, Goudi, Athens, Greece

Received 27 March 2006; received in revised form 10 May 2006; accepted 18 May 2006

Available online 30 June 2006

## Abstract

X-ray absorption and X-ray fluorescence properties of medical imaging scintillating screens were studied by Monte Carlo methods as a function of the incident photon energy and screen-coating thickness. The scintillating materials examined were Gd<sub>2</sub>O<sub>2</sub>S, (GOS) Gd<sub>2</sub>SiO<sub>5</sub> (GSO) YAlO<sub>3</sub> (YAP), Y<sub>3</sub>Al<sub>5</sub>O<sub>12</sub> (YAG), LuSiO<sub>5</sub> (LSO), LuAlO<sub>3</sub> (LuAP) and ZnS. Monoenergetic photon exposures were modeled in the range from 10 to 100 keV. The corresponding ranges of coating thicknesses of the investigated scintillating screens ranged up to 200 mg cm<sup>-2</sup>. Results indicated that X-ray absorption and X-ray fluorescence are affected by the incident photon energy and the screen's coating thickness. Regarding incident photon energy, this X-ray absorption and fluorescence was found to exhibit very intense changes near the corresponding K edge of the heaviest element in the screen's scintillating material. Regarding coating thickness, thicker screens exhibited higher X-ray absorption and X-ray fluorescence. Results also indicated that a significant fraction of the generated X-ray fluorescent quanta escape from the scintillating screen. This fraction was found to increase with screen's coating thickness. At the energy range studied, most of the incident photons were found to be absorbed via one-hit photoelectric effect. As a result, the reabsorption of scattered radiation was found to be of rather minor importance; nevertheless this was found to increase with the screen's coating thickness. Differences in X-ray absorption and X-ray fluorescence were found among the various scintillators studied. LSO scintillator was found to be the most attractive material for use in many X-ray imaging applications, exhibiting the best absorption properties in the largest part of the energy range studied. Y-based scintillators were also found to be of significant absorption performance within the low energy ranges.

© 2006 Elsevier B.V. All rights reserved.

PACS: 02.70.Uu; 29.40.-n; 87.59.Bh

Keywords: Scintillators; Monte Carlo; X-ray imaging; Radiation detectors

## 1. Introduction

Scintillator-based radiation detectors have been rapidly developed during the last few decades for application in conventional and digital medical imaging such as conventional and digital X-ray radiography or fluoroscopy, X-ray computed tomography, single-photon emission tomogra-

phy (SPECT) and positron emission tomography (PET). In most cases, scintillators are coupled to optical sensors, such as films, photocathodes, photodiodes, amorphous silicon and thin film transistor technology (a-Si/TFTs), charged coupled devices (CCDs) and complementary metal oxide semiconductors (CMOS) [1–7]. Because of differences in detector design in various medical imaging modalities, and considering the constraints of cost, durability, image quality and patient dose burden, the interest in developing new scintillator materials, exhibiting adequate radiation detection properties, has been renewed [8].

\*Corresponding author. Tel.: +3010 5385375; fax: +3010 5910975.

E-mail addresses: [dniko@teiath.gr](mailto:dniko@teiath.gr) (D. Nikolopoulos), [kandarakis@teiath.gr](mailto:kandarakis@teiath.gr) (I. Kandarakis).

In designing and evaluating scintillator-based radiation detectors, it is of importance to accurately determine the radiation detection efficiency of the built-in scintillator. Depending on the imaging application this efficiency has been expressed by the quantum absorption efficiency or the energy absorption efficiency [9]. Issues, such as the amount of emission and reabsorption of scattered and characteristic X-ray fluorescence radiation, and that of Auger electron energy, are of great importance. When scattered or characteristic radiation is reabsorbed within the scintillator, apart from the primary interaction point, a loss of spatial resolution and image contrast may occur [9]. On the other hand, if this type of radiation escapes the detector, radiation detection efficiency may be reduced.

Radiation transport phenomena have been extensively studied by application of the Monte Carlo technique. This was proven to be by far the most successful technique for the simulation of the stochastic processes involved in radiation detection [10]. During the last decade, various Monte Carlo simulation packages have become commercially available. Some research groups have reported results on application of such packages in studies of photon transport phenomena in scintillators employed in X-ray medical imaging [8,9,11]. However, the commercially available Monte Carlo simulation packages are of general-purpose design [12–15]. Thus, their application is constrained by their expediency and feasibility in specializing to firm situations. In addition, the most popular packages i.e. EGS, TART, GEANT and PENELOPE, have been developed and verified for studies mainly in the field of nuclear and high-energy physics [12–15], i.e. for energies outside the range of energies employed in mammography and general radiology.

In this consensus, the present paper aims at the development of expedite and feasible Monte Carlo simulation codes focused to the study of photon transport, photon absorption and X-ray fluorescence generation phenomena occurring in scintillators employed, in ordinary X-ray medical imaging modalities (general conventional and digital radiography–fluoroscopy and computed tomography). In addition, this paper aims at applying the developed codes to the investigation of X-ray absorption properties of various new scintillator materials so as to examine their suitability for use in various X-ray medical imaging applications.

Accordingly, certain simulation Monte Carlo codes have been developed which were applied to the investigation of absorption properties of five new scintillators. Particular interest was paid on the contribution of the generation, reabsorption or escape of K- and L-characteristic photons, on these properties. The new scintillators studied were  $\text{YAlO}_3$  (YAP),  $\text{Y}_3\text{Al}_5\text{O}_{12}$  (YAG),  $\text{LuSiO}_5$  (LSO),  $\text{LuAlO}_3$  (LuAP) and  $\text{Gd}_2\text{SiO}_5$  (GSO). With the exception of the LuAP scintillator, all other scintillators are available in powder form, and thus, they could be considered for use in X-ray imaging applications. The LuAP scintillator, however, was also included because of its relevance to both

LSO and YAP scintillators. All these scintillators were modeled and their absorption properties were studied as a function of incident photon energy and screen coating thickness. In addition, the well-known  $\text{Gd}_2\text{O}_2\text{S}$  (GOS) X-ray imaging scintillator and the traditional ZnS, used in a variety of imaging and non-imaging applications [3,7,9], were also included in the study for comparison purposes.

## 2. Materials and methods

### 2.1. Monte Carlo codes

The Monte Carlo codes were developed using the Microsoft FORTAN Developer PC platform. The codes were designed so as to be efficient for applications in the photon energy range employed in medical X-ray imaging and easily adjustable to various scintillator materials.

Photon transport modeling was based on the three processes governing photon interactions in the medical X-ray imaging energy range i.e. coherent–incoherent scattering and photoelectric absorption. An iterative procedure was used; a photon of certain energy was generated and considered to hit the entrance surface of a scintillator screen of predefined dimensions under known direction angles. Using random numbers and cross-sectional data, the mean free photon path, as well as the site and type of the subsequent photon interaction were determined. In the case of scatter and by employing a method proposed by Chan and Doi [10,16], based on the use of the form and scatter factors of the materials under study, the photon transport parameters were calculated, i.e. photon energy and direction angles after the interaction and energy transferred to the electrons of the medium. The cross-sections of the scintillator materials under study were calculated using the XCOM code, which was based on the tables of Hubbell and Seltzer [17]. The XCOM code was downloaded from the NIST reference database [18]. The form factors and the scatter factors of the scintillator materials under study were calculated from those corresponding to the elements constituting these scintillator materials using specially designed codes. The factors for the elements were also downloaded from the NIST reference database [19]. The iterative procedure was continued until the photon escaped from- or was absorbed within, the scintillator block. In the latter case, all energy of the photon was considered to be transferred to the medium except a part, which was considered to refer to the generation of characteristic fluorescence radiation or Auger electrons. Selection between characteristic fluorescence radiation and Auger electrons was based on a random-number generation routine. In the case of characteristic fluorescence radiation simulation, photons were modeled as independent K- or L-characteristic quanta initiating their history at the photoelectric interaction site. The histories of the characteristic photons were followed similar to those of the primary ones. The characteristic fluorescence photons were generated with a uniform distribution

of the azimuthal angle. In the case of Auger electron production simulation, the part of the energy referring to Auger electrons was considered to be completely transferred to the scintillator block at the site of interaction.

Various Monte Carlo simulation runs were performed. In every run  $10^7$  photons were generated and traced. All photon track and energy histories were recorded for further analysis.

Before proceeding in further simulations and for purposes of comparison to published data derived by well validated Monte Carlo codes, certain runs concerning water phantoms were performed. First, following the work of Boone [20], the depth of energy deposition in water was assessed for three monoenergetic X-ray beams (15, 20, 30 keV). A water slab of 10 cm thickness and of infinite area was simulated. Exposure was modeled as a narrow beam of photons normally impinging on the slab. The energy deposited (in keV/cm) in slabs of varying depths was calculated. The calculated values were similar to the reported values by Boone [20], except for the values corresponding to a 15 keV beam, for which a more rapid drop with increasing depth was found. Agreement within  $\pm 10\%$  was achieved. For example, at 15 keV the energy deposition (keV/cm) at 6 cm found by Boone [20] was 0.25 keV/cm while the present code gave 0.24 keV/cm. At 20 keV and 6 cm, these values were 8.2 and 8.8 keV/cm, and, at 30 keV and 1 cm, the corresponding values were 1.9 and 1.2 keV/cm. Second, following the work of Chan and Doi [21], the spatial distribution of the relative energy absorption, due to scattered radiation, was calculated in a 10 cm thick water phantom, for incident X-rays of 100 keV energy impinging at pencil beam geometry. Agreement within  $\pm 12\%$  was achieved. For example, at the depth of 8–9 cm at 2 cm distance from the center, the reported value was 0.36 while the present code gave 0.35. At the depth of 4–5 cm and at distance 1 cm, the above values were 0.40 and 0.41, respectively. Third, following the work of Chan and Doi (1986) [22], a water slab with thicknesses of 5, 10, 15 and 20 cm, irradiated by a monoenergetic narrow beam of photons of various energies, was modeled. The mean number of interactions for each incident photon was determined and compared to published data. Agreement within  $\pm 3\%$  was achieved. For example, for the 20 cm phantom at 50 keV exposures, the reported value was approximately 3.5 while our code gave 3.6. At 100 keV, this value was 5.2.

## 2.2. Modeled scintillators

The new scintillating materials (YAP, YAG, LSO, LuAP and GSO) are often doped with cerium (Ce) activator, which induces a very fast decay time (20–70 ns)[7,23–28]. These materials have not yet been used in medical X-ray imaging, however due to some of their intrinsic physical properties, they could be considered for use in such applications. Yttrium-based (YAP and YAG) scintillators are of medium to low density (5.37 and 4.15 g cm<sup>-3</sup>

respectively) and of relatively low effective atomic number. However their optical emission spectra, when doped with Ce activator, are compatible with the spectral sensitivity curves of existing optical detectors [7,23–25]. Up to now YAP and YAG have been employed in a variety of applications from positron imaging (YAP) to electron microscopy (YAG) and low-energy nonimaging X-ray radiation detectors (YAG) [28]. Gadolinium (GSO) and Lutetium (LSO, LuAP)-based materials have been used (GSO, LSO), or have been studied for use, in positron imaging [7]. These scintillators are very attractive for X-ray medical imaging applications due to their high effective atomic number and density. On the other hand, GOS is a well-known efficient scintillator, which has been used in a large variety of X-ray imaging applications such as conventional radiography (Gd<sub>2</sub>O<sub>2</sub>S: Tb), digital radiography (Gd<sub>2</sub>O<sub>2</sub>S:Tb, Gd<sub>2</sub>O<sub>2</sub>S:Eu) and X-ray computed tomography (Gd<sub>2</sub>O<sub>2</sub>S:Pr or Gd<sub>2</sub>O<sub>2</sub>S:Pr, Ce, F) [26,27]. ZnS is a traditional scintillator exhibiting very high intrinsic conversion efficiency ( $\sim 25\%$ ), which has been used in various image display units, in fluoroscopic image intensifiers and in many nonimaging radiation detection applications (ZnS:Ag, ZnS:Cu etc.) [7].

## 2.3. Detector parameters studied

The main detector parameters studied were the efficiency of absorption of incident energy (EAIE) and the quantum absorption efficiency (QAE).

The EAIE of a scintillator is defined as the fraction of the energy of photons totally absorbed within a scintillator block over the total incident energy. EAIE includes all mechanisms of energy deposition within the scintillator's mass. EAIE is a measure of the absorbed energy and represents the efficiency of a detector to capture the useful X-ray-imaging signal [10,29,30]. The EAIE was classified into the following classes:

- (a) Overall absorbed-EAIE: energy absorbed due to all types of absorption mechanisms, i.e., photoelectrons ejected after a photoelectric effect, electrons ejected after a Compton event, and Auger electrons ejected after X-ray fluorescence transitions following a photoelectric effect. This class was accompanied by two additional classes: (i) overall-AF-EAIE: considering that all fluorescence (AF) radiation was completely absorbed within the scintillator, and (ii) overall-NF-EAIE: considering that no fluorescence (NF) radiation was absorbed within the scintillator and as a result it escaped.
- (b) Scattered and reabsorbed-EAIE: energy absorbed after one or multiple scattering events of the primary photons.
- (c) Fluorescence generated: energy transferred to characteristic fluorescence quanta following a photoelectric effect.
- (d) Fluorescence reabsorbed: fluorescence-generated-EAIE, which was absorbed within the scintillator.

Two additional classes related to EAIE were considered:

- (e) escaped incident energy fraction: energy escaped from the scintillator block.
- (f) Fluorescence escaped: the fraction of incident energy corresponding to absorbed photons producing fluorescence radiation escaping the scintillator.

In all classes, the energy transferred to the ejected electrons was considered to be fully absorbed at the site of ejection.

QAE was defined as the number of the totally absorbed photons within a scintillator block over the total number of incident photons [10,29,30]. QAE was accompanied by an additional class: QAE-photoelectrically absorbed; via one-hit photoelectrical event. Two additional classes were also considered, corresponding to detected and nondetected characteristic fluorescence radiation produced after photoelectric absorption of incident photons: (a) QAE-fluorescence forward escaped; characteristic quanta escaped from the scintillator in the forward direction and (b) QAE-fluorescence backscattered; characteristic quanta from the scintillator in the backward direction.

#### 2.4. Simulated detector design

The physical characteristics of each scintillator under study are given in Table 1. The scintillators were modeled as blocks in the form of granular scintillating screens i.e. screens containing luminescent grains within a binding material. These screens were of  $35 \times 43 \text{ cm}^2$  entrance area and of varying coating thickness expressed in coating weight units ( $\text{mg cm}^{-2}$ ). The physical densities of the scintillators were thus used to adjust the actual thicknesses appropriately. A 50–50% scintillator–binder combination was taken into account.

The studied detector parameters were investigated as a function of incident photon energy over constant coating thickness and as a function of coating thickness. In examining the role of photon energy, two coating thickness values were investigated; that of  $80 \text{ mg cm}^{-2}$  and that of  $100 \text{ mg cm}^{-2}$ . Both thickness values were considered as representative for radiographic imaging [29]. In examining

the role of coating thickness, monoenergetic incident photons of 20 and 65 keV energy were considered. The 20 keV energy was considered as typical for mammographic applications. The 65 keV one is well within the energy range used in general X-ray radiography applications. A series of thickness values ranging up to  $200 \text{ mg cm}^{-2}$  were in this case investigated.

#### 2.5. Simulated X-ray detector exposures

Modeled scintillators were considered to be exposed to X-rays initiating from a point source located at the central axis of the entrance area of the scintillator block. Photons were generated within a field. Source to scintillator block distance and field size at the entrance surface were defined at the beginning of each Monte Carlo run, together with the energy of the emitted X-ray quanta. This energy was constant for modeling monoenergetic X-ray detector exposures. The direction angles of the emitted photons were defined by the source to scintillator block distance and the field size dimensions at entrance area, using random numbers. Normal photon incidence was simulated considering zero dimensions of this area. In all cases, X-rays were generated in normal incidence onto the scintillator.

### 3. Results and discussion

Figs. 1 and 2 show the incident photon energy redistribution ways within or through a scintillating screen under study. Fig. 1 presents the EAIE of the primary radiation, while Fig. 2 the EAIE of the fluorescence radiation produced as a result of X-ray energy deposition within the scintillating screen. To avoid confusion, only data corresponding to the GSO, LSO and YAP  $100 \text{ mg cm}^{-2}$  screens are presented in each figure. Curves obtained for the other screens were of similar shape. The figures present the various classes defined earlier in the text.

The overall absorbed-EAIE of every scintillator studied, decreases with incident photon energy up to the value of the corresponding K-photoelectric absorption edge of the heaviest element in the scintillator material. At this K-edge energy, the overall absorbed-EAIE was found to exhibit a step increase. This is due to the sudden increase of photoelectric absorption events occurring at this K shell. Thereafter, the overall absorbed-EAIE was found to continuously decrease. For the case of ZnS scintillator this step increase lies at relatively low energy (9.659 keV).

The overall absorbed-EAIE of the  $80 \text{ mg cm}^{-2}$  coating thickness scintillating screens, although not presented, was found to be lower than that of the  $100 \text{ mg cm}^{-2}$  ones, in the whole energy range studied. This difference was found to depend on incident photon energy.

At the energy range studied, scatter and reabsorbed-EAIE was found to be below 3% of the maximum EAIE for every investigated scintillating screen. Consequently,

Table 1  
Physical characteristics of the scintillators studied

	Density ( $\text{g cm}^{-3}$ )	High-Z Element and K energy (keV)
YAlO <sub>3</sub> (YAP)	5.37	Y : Z = 39, K = 17.038
Y <sub>3</sub> Al <sub>5</sub> O <sub>12</sub> (YAG)	4.15	Y : Z = 39, K = 17.038
LuSiO <sub>5</sub> (LSO)	7.40	Lu: Z = 71, K = 63.316
LuAlO <sub>3</sub> (LuAP)	8.30	Lu: Z = 71, K = 63.316
Gd <sub>2</sub> SiO <sub>5</sub> (GSO)	6.71	Gd: Z = 64, K = 50.239
Gd <sub>2</sub> O <sub>2</sub> S (GOS)	7.34	Gd: Z = 64, K = 50.239
ZnS	4.09	Zn: Z = 30, K = 9.659

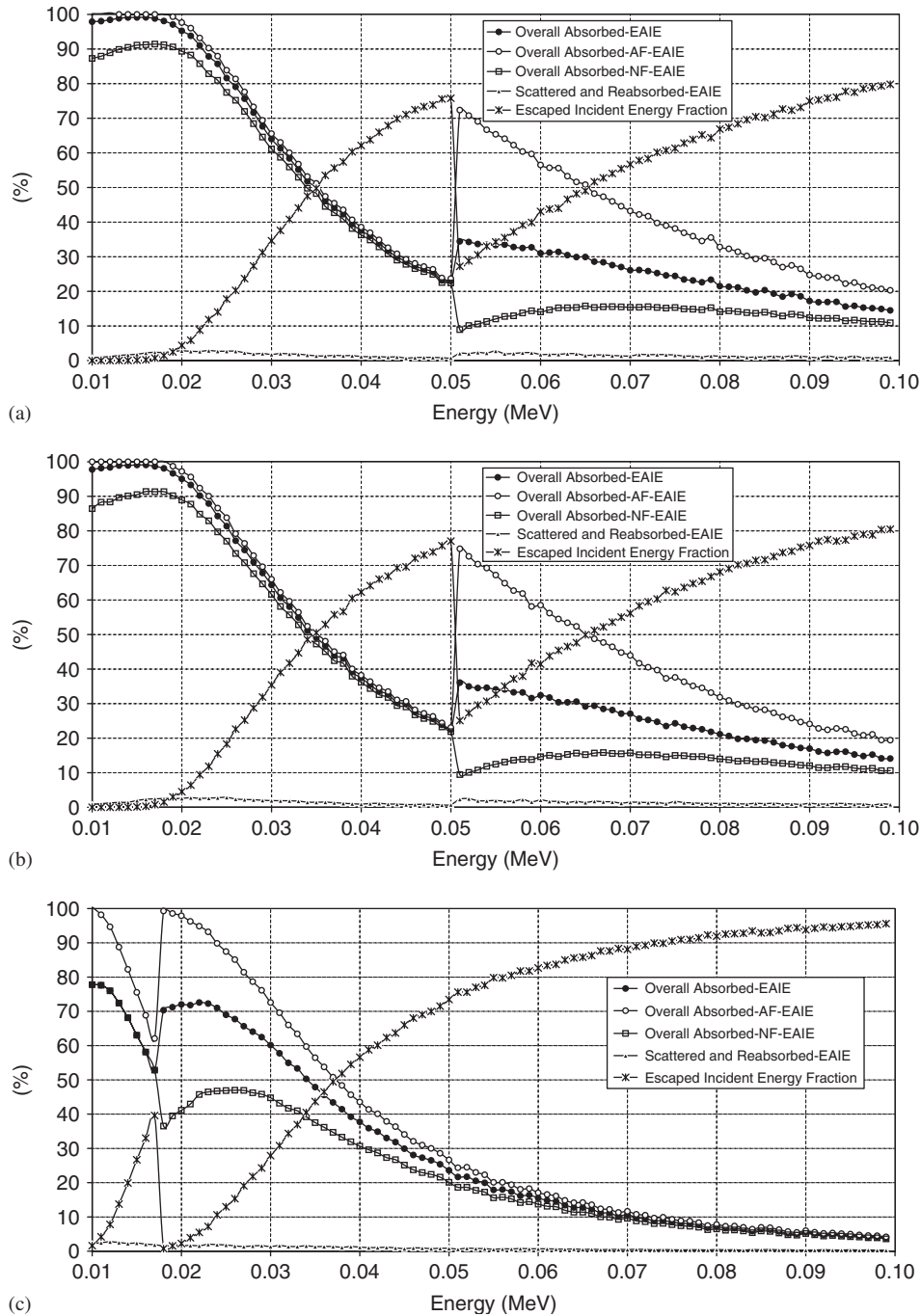


Fig. 1. Dependence of EAIE of the investigated scintillators as a function of incident photon energy: (a) GSO, (b) LSO and (c) YAG.

the incident photons are absorbed mainly via one-hit photoelectric effect.

Differences between the shapes of the overall absorbed-EAIE curves of the investigated scintillating screens were observed. For the gadolinium-based scintillators (GOS and GSO) and for energies below 20 keV, the overall absorbed-EAIE was found to be between 99% and 95%. Just below the Gd K edge (50.239 keV), this value was found to be 23% for the GOS and 22% for the GSO scintillator. Above this K edge these values increased abruptly to 36% and

34%, respectively. Thereafter they continued to fall, down to 14% for both scintillators at 100 keV. For the lutetium-based scintillators and for energies up to 15 keV the overall absorbed-EAIE was between 97% and 99% for LSO and between 96% and 98% for LuAP. The overall absorbed-EAIE was found to fall continuously, both for LSO and LuAP, down to 17% just below the Lu K edge (63.316 keV). Above this edge it was found to increase to 24% for LSO and 23% for LuAP and to fall down to 15% at 100 keV. Particularly, the LuAP scintillator was found to

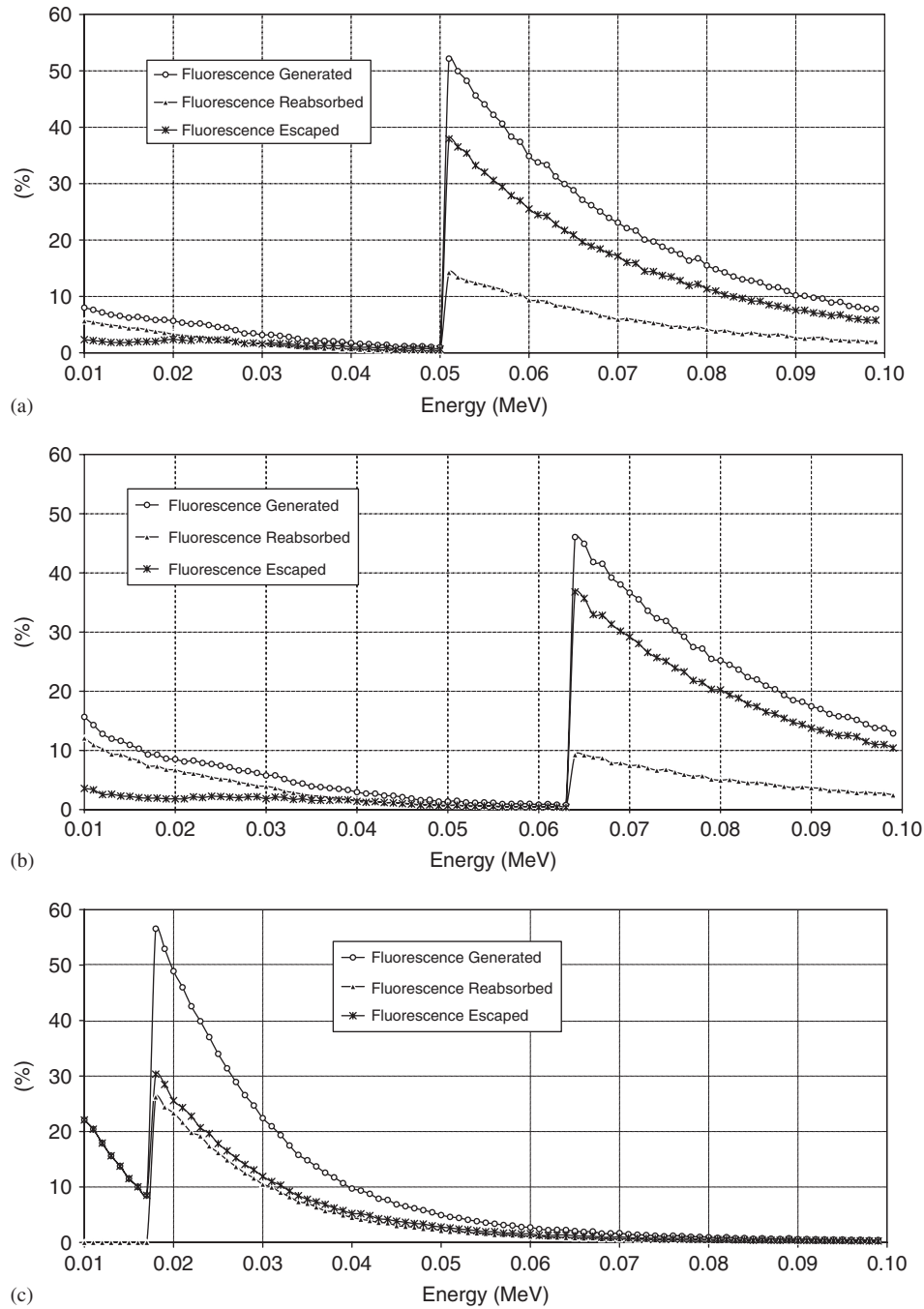


Fig. 2. Dependence of fluorescence EAIE of the investigated scintillators as a function of incident photon energy: (a) GSO, (b) LSO and (c) YAG.

exhibit an increase of higher intensity near the Lu K edge beginning slightly before the corresponding Lu K edge. The overall absorbed-EAIE of the yttrium-based scintillators, was found to fall down from 78% to 53% for YAG and 49% for YAP just below the yttrium K edge (17.038 keV). Just above this K edge it was 70% for YAG and 67% for YAP, respectively. Thereafter, it was found to fall continuously down to 3% at 100 keV for both scintillators. The overall absorbed-EAIE of the ZnS scintillating screen was found to increase from 82% at

10 keV to 91% at 15 keV and to fall continuously thereafter down to 2% at 100 keV.

As can be seen from Fig. 1, the overall-AF-EAIE and the overall absorbed-EAIE of the investigated scintillating screens were found comparable for energies, relatively near but below, the corresponding K edge. This was also observed for the modeled scintillating screens not presented in Fig. 1. The contribution to the overall absorbed-EAIE of the fluorescence radiation generated, at these energies, mainly in the L shells, is negligible. This is more

demonstratively shown in Fig. 2 where the fluorescence-generated-EAIE and fluorescence-reabsorbed-EAIE values presented, are almost negligible at the corresponding energies. In the rest of the energy range studied, the overall-AF-EAIE and the fluorescence-generated-EAIE values are higher than the corresponding overall absorbed-EAIE and the fluorescence-reabsorbed-EAIE. This was also found valid for the scintillating screens not presented in Fig. 2. Accordingly, a fraction of the generated fluorescence photons escape the scintillating screen. This fraction depends on the scintillating screen material and on the incident photon energy. The differences between the overall-AF-EAIE and the fluorescence-generated-EAIE compared to corresponding values of the overall absorbed-EAIE and the fluorescence-reabsorbed-EAIE are due to the fluorescence-escaped-EAIE. The fluorescence-escaped-EAIE contribution is more significant for energies above the corresponding K edge but its contribution is fading with increasing energy. Noticeable is the fact that this contribution is rather stable and below 1% as the energy decreases below the corresponding K-edge. Of significance to note is that the majority of L- and lower-S shell characteristic fluorescence photons generated are finally, more or less, absorbed within the scintillating screen.

For all of the investigated scintillating screens, the fluorescence generated-EAIE was found to decrease up to the corresponding K edge, to exhibit a very sudden increase at this K edge and to continue to decrease up to 100 keV. Similar curve shapes were found both for the fluorescence reabsorbed-EAIE and the fluorescence escaped-EAIE; the latter for energies above the corresponding one of the K edge.

Variations in fluorescence-generated-EAIE, fluorescence-reabsorbed-EAIE and fluorescence-escaped-EAIE were observed between the various scintillating screens. For the gadolinium-based scintillators, fluorescence-generated-EAIE and fluorescence-reabsorbed-EAIE were approximately 1% for both scintillators just below the Gd K edge (50.239 keV). Just above this K edge the fluorescence-generated-EAIE was 54% for GOS and 52% for GSO, while the fluorescence-reabsorbed-EAIE was 39% for GOS and 38% for GSO respectively. For the Lutetium-based scintillators the fluorescence-generated-EAIE was 1% below the corresponding Lu K edge, while 46% for LSO and 44% for LuAP just above this edge. The fluorescence-reabsorbed-EAIE was 1% below the corresponding Lu K edge and 37% for LSO and 35% for LuAP just above. For the yttrium-based scintillators and just below the corresponding Y K edge, the fluorescence-generated-EAIE was 8% for YAG and 9% for YAP, while the fluorescence-reabsorbed-EAIE was negligible for both scintillators. Just above this K edge, the fluorescence-generated-EAIE was 57% for YAG and 55% for YAP, while the fluorescence-reabsorbed-EAIE was 30% for YAG and 29% for YAP, respectively. For the ZnS scintillator both parameters were found to continuously

fall from 42% and 24% at 10 keV, respectively, to negligible values at approximately 70 keV.

In the energy range below the corresponding K edge energies and for all of the investigated scintillating screens, the values of the fluorescence-generated-EAIE and the fluorescence-reabsorbed-EAIE, both corresponding to L- and lower-shell fluorescence characteristic photons, were significantly lower than the corresponding values above this K edge. These results indicate that the contribution of the fluorescence radiation to the overall absorbed-EAIE is mainly due to K-characteristic photons. Similar results are also reported by others [8,29]. These issues indicate also that, above K edge, a significant part of the overall absorbed-EAIE is due to reabsorption of K-characteristic fluorescence radiation. Similar results reported by others were in close agreement [8,21,29,31,32].

Scatter and reabsorbed-EAIE presented discrepancies among the various scintillating screens and the various scintillator thicknesses studied. Generally, the scatter and reabsorbed-EAIE increases with screen thickness. Noticeable is that the scatter and reabsorbed-EAIE of the Gd- and Lu-based screens exhibited a local maximum at 25–30 keV. This local maximum is related to the increased probability of coherent scattering in that energy range. In every case, the scatter and reabsorbed-EAIE was found to fall with increasing energy up to 100 keV mainly because the overall absorbed-EAIE was falling with increasing energy, accordingly.

The QAE of the investigated scintillators is presented in Fig. 3. For energies above the energy of the corresponding K edges, QAE and QAE-photoelectrically absorbed were almost equal. This is related to the fact that the investigated scintillators absorb photons mainly via one-hit photoelectric effect. For lower energies QAE-photoelectrically absorbed was slightly lower than QAE. This is related mainly to coherent scattering. In every case the QAE presents a continuous decrease down to the energy of the K edge, sudden increase and continuous decrease down to the end of the investigated energy range. Since the modeled exposures were monoenergetic, QAE followed the variations of the overall absorbed-EAIE.

It is of significance to note that for incident photon energies higher than approximately 40 keV QAE-forward escaped and QAE-backscattered are almost equal. On the other hand for lower incident photon energies the QAE-backscattered is significantly higher than the QAE-forward escaped. This fact is jointly related both to the emission and the absorption of the characteristic photons generated within the scintillating screen. On the one hand, the emission of fluorescence photons is isotropic and therefore, the probabilities of forward and backward direction are equal. On the other hand, depending on the generation depth, the escape probabilities of the forward- and backward-directed characteristic quanta are different. In particular, the majority of incident photons are absorbed at low depths within the scintillating screen and hence, the

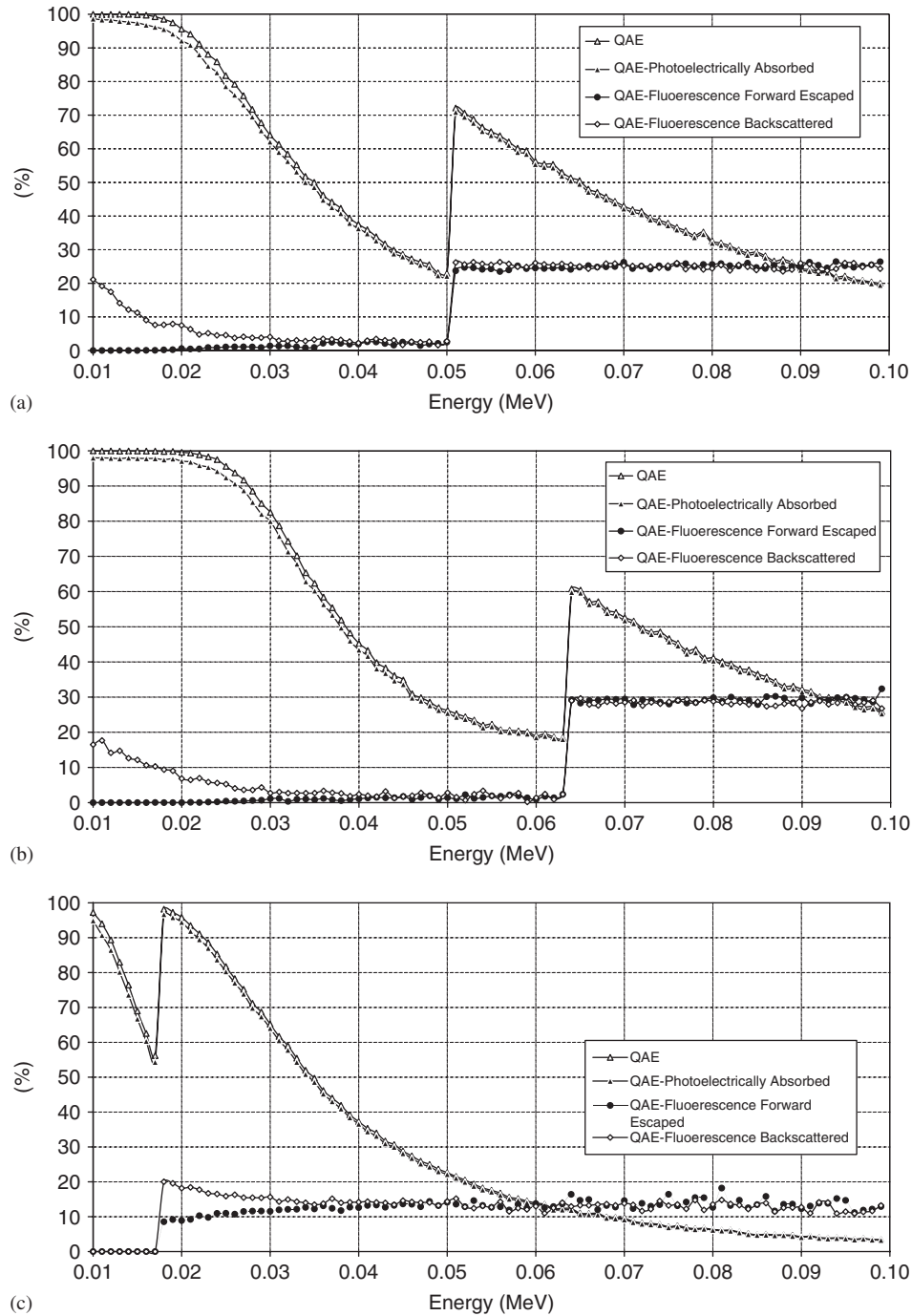


Fig. 3. Dependence of QAE of the investigated scintillators as a function incident photon energy: (a) GSO, (b) LSO and (c) YAG.

corresponding fluorescence photons directed backwards are more easily transmitted through, since they have to travel shorter distances. As a result, the backward escape of fluorescence photons is pronounced. This is a possible reason explaining the higher values of QAE-backscattered at low incident photon energies. However, when incident photon energy increases incident photons are more penetrating, fluorescence photons are generated deeper

within the scintillating screen and forward escape of these fluorescence photons gradually compensates the pronounced backward escape. This could provide an explanation why QAE-forward escaped and QAE-backscattered are almost equal at high incident photon energies. This is also reinforced, by the fact that both forward- and backward-directed characteristic quanta are easily transmitted through the scintillating screen, since the energies of

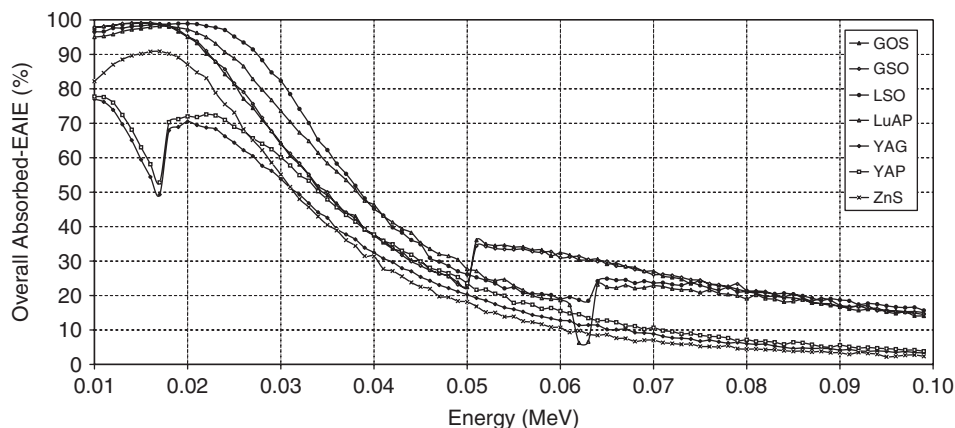


Fig. 4. Dependence of EAIE values of the investigated scintillators as a function incident photon energy.

these quanta are just below the ionization energy levels (K, L or lower) and thus their absorption is low. These reported results are in close agreement with results reported by others concerning GOS and other scintillating materials at comparable coating thicknesses [9].

A comparison between the various scintillating screens is shown in Fig. 4. At the very low energy range up to the Y K-edge energy (17.038 keV), GSO scintillator was found to exhibit the highest overall absorbed-EAIE. In the very interesting for mammographic applications energy range, from 17 keV up to 22 keV, the scintillators based on Lu (LuAP, LSO) and on Gd (GOS, GSO) were found to present the highest overall absorbed-EAIE values; nevertheless all these being comparable to each other. In the low energy range from 21 to 40 keV, which is interesting for low energy X-ray general radiography applications, the LSO scintillator was found to present the highest overall absorbed-EAIE. In this range, LuAP scintillators presented higher values of the overall absorbed-EAIE than those corresponding to the GOS scintillator. These were higher than those corresponding to the GOS scintillator. In this energy range, the overall absorbed-EAIE of the GSO and YAG scintillators yet being comparable to each other, were lower than the GOS ones. In the energy range from 40 keV up to the Gd K-edge energy (50.239 keV), which is interesting for general diagnostic radiology, LSO, GOS and YAP scintillators presented comparable values of the overall absorbed-EAIE. However, all these values were lower than the LuAP ones. GSO and YAG scintillators continued to present comparable values of this EAIE class, which were all lower than the LSO, GOS and YAP values. Above the K-edge energy of Gd up to the corresponding one of Lu, GOS and GSO scintillators present comparable overall absorbed-EAIE values which are exceptionally higher than the ones of all other scintillators. In the energy range, interesting for general radiography, fluoroscopy and computed tomography, beginning from the K edge energy of Lu and ending to 100 keV, the LSO scintillator was again found to present the highest overall absorbed-EAIE.

In comparison, the overall absorbed-EAIE values of GOS, GSO and LuAP scintillators, yet comparable to each other, were all found to be lower. The ZnS scintillator presented the lowest overall absorbed-EAIE in the energy range from 22 keV and thereafter.

Figs. 5 and 6 show the variations of EAIE parameters studied with coating thickness. For every screen, the overall absorbed-EAIE was found to increase with screen coating thickness due to the resulting increase in the probability of incident photon absorption. The fluorescence-generated-EAIE and accordingly the fluorescence-reabsorbed-EAIE were also found to increase with screen coating thickness. This is due to the corresponding increase in the overall absorbed-EAIE. At the studied thickness range, the fluorescence-escaped-EAIE for the scintillators based on Lu (LuAP, LSO) and on Gd (GOS, GSO) was found to increase with coating thickness, but at a lower rate. On the other hand, the fluorescence-escaped-EAIE for the scintillators based on Y (YAG and YAP) at the 20 keV simulated exposure was found to decrease after a plateau value at the thickness of  $50 \text{ mg cm}^{-2}$ . This is due to the gradual increase of the fluorescence-reabsorbed-EAIE increasing rate with coating thickness. Scatter and reabsorbed-EAIE also increased with coating thickness. This is due to the higher probability of scatter in a thicker scintillator. On the other hand, the escaped incident energy fraction was found to decrease with scintillator coating thickness. This is due to the increase in the overall absorbed-EAIE. Depending on the scintillator material all these parameters show higher values either for the 65 keV or the 20 keV simulated exposures.

As pointed out from certain calculations, which for brevity are not shown in the figures, the fraction of the scatter and reabsorbed-EAIE over the overall absorbed-EAIE, was found to be very slightly increasing with coating thickness for all of the investigated screens both for 20 and 65 keV simulated exposures. This is due to the fact that, in the investigated thickness range, Compton scattering is

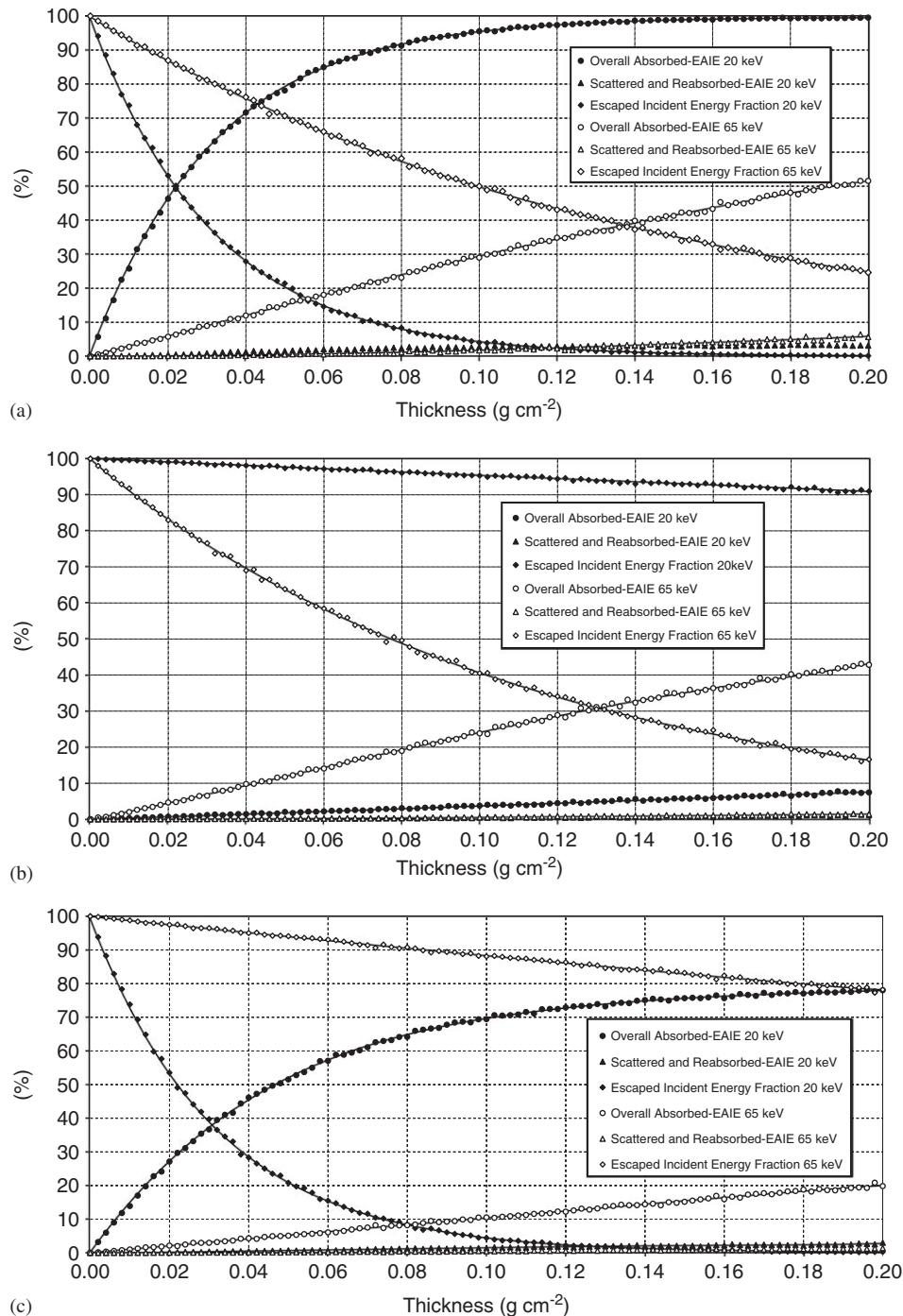


Fig. 5. Dependence of EAIE of the investigated scintillators as a function screens coating thickness: (a) GSO, (b) LSO and (c) YAG.

slightly more probable to occur in thicker scintillators. This fraction was found to be significantly higher for the 65 keV simulated exposures compared to the 20 keV ones. This is due to the fact that, for 65 keV, Compton scattering is more probable to occur.

Out of some additional calculations, a similar fraction was also calculated but again not shown for brevity. This was the fraction of fluorescence-generated-EAIE over the

overall-absorbed-EAIE. This fraction was found to be fairly constant with coating thickness for all investigated scintillators and for all simulated exposures. This fraction was also found to be very higher for the 65 keV simulated exposures, because in these, in addition to the L- and lower-shell fluorescence photons generated at 20 keV, K characteristic are also generated and with a very higher yield [22].

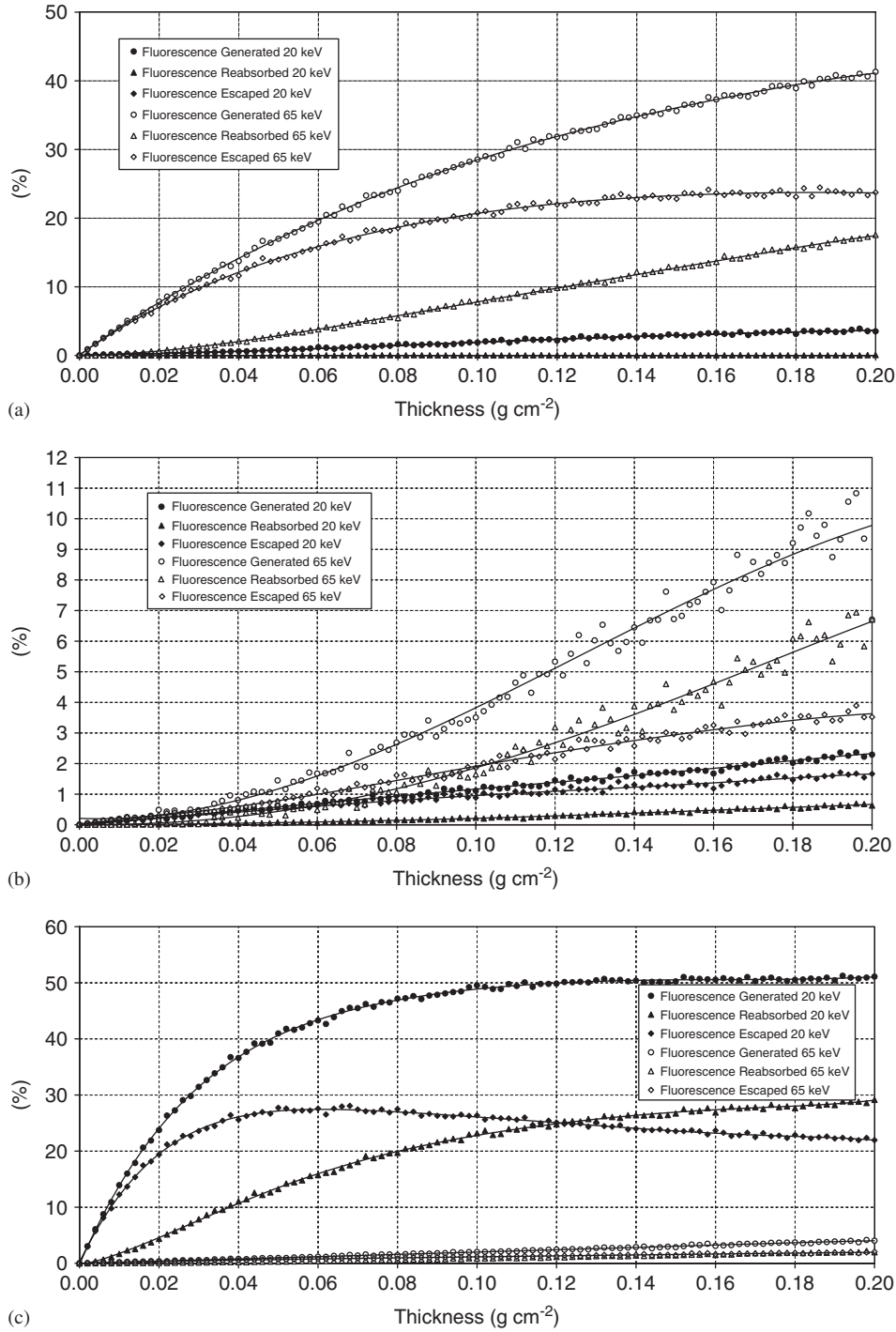


Fig. 6. Dependence of fluorescence EAIE of the investigated scintillators as a function of screens coating thickness: (a) GSO, (b) LSO and (c) YAG.

Fig. 7 shows a comparison between the various scintillators studied. Gd- and Lu-based scintillators absorb better with increasing thickness.

In conclusion, at the energy range studied, most of the primary X-ray quanta were found to be absorbed photoelectrically, after one-hit effect. Consequently, reabsorption of scattered radiation was found to be of minor significance. Significant variations depending on incident

X-ray energy and scintillator thickness among the various investigated scintillators were observed. LSO scintillator was found to be the scintillating material most suitable for use in many X-ray imaging applications, exhibiting the best absorption properties in the largest part of the energy range studied. Gd-based scintillators were also found of importance regarding their X-ray absorption performance, especially within the low-energy ranges.

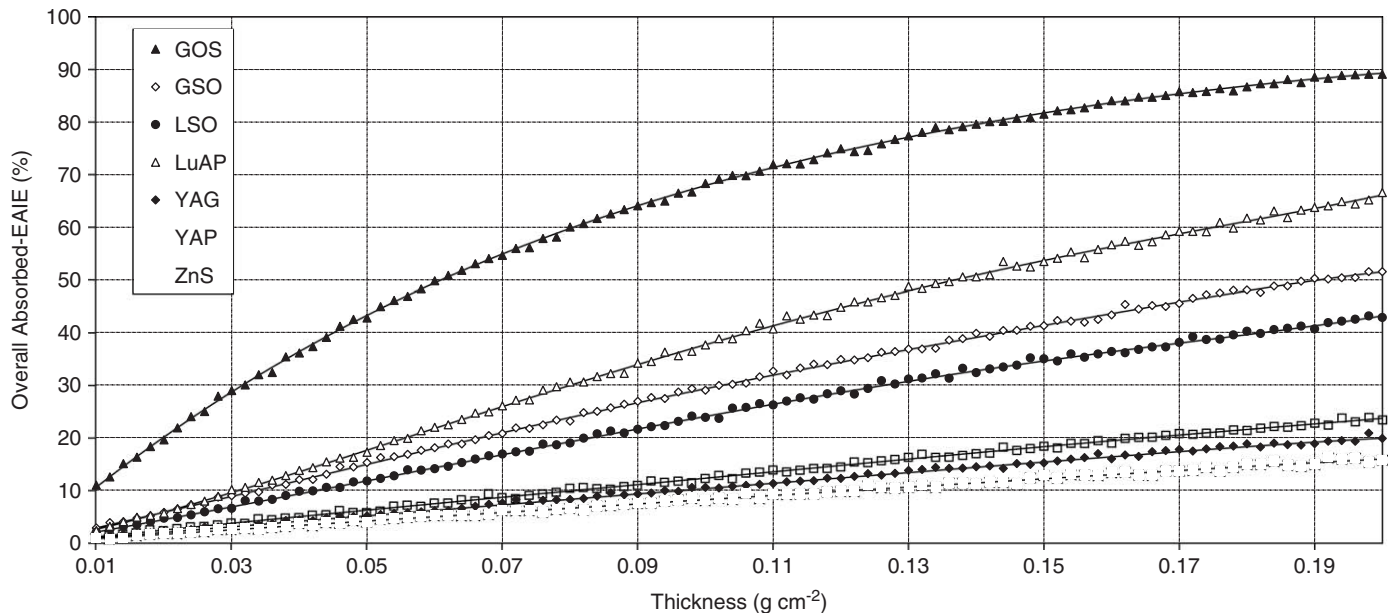


Fig. 7. Dependence of EAIE values of the investigated scintillators as a function thickness.

## Acknowledgements

This work was financially supported by the Greek Ministry of Education (program EPEAEK “Archimidis”).

## References

- [1] S. Hejazi, D.P. Tauernicht, *Med. Phys.* 24 (1997) 287.
- [2] T. Yu, J.M. Sabol, J.A. Seibert, J.M. Boone, *Med. Phys.* 24 (1997) 279.
- [3] H.J. Besch, *Nucl. Instr. and Meth. A* 419 (1998) 201.
- [4] T.T. Farman, A.G. Farman, *J. Digit. Imaging* 11 (1998) 169.
- [5] J.H. Siewersden, L.E. Antonuk, Y. el-Mohri, J. Yorkston, W. Huang, V.E. Scarpine, R.A. Street, *Med. Phys.* 24 (1997) 51.
- [6] E. Hell, W. Knüpfner, D. Mattern, *Nucl. Instr. Meth. A* 454 (2000) 40.
- [7] C.W.E. van Eijk, *Phys. Med. Biol.* 47 (2002) R85.
- [8] J.M. Bonne, V.N. Cooper, *Med. Phys.* 27 (8) (2000) 1818.
- [9] J.M. Boone, J.A. Seibert, J.M. Sabol, M. Tecotzky, *Med. Phys.* 26 (6) (1999) 905.
- [10] H.P. Chan, K. Doi, *Phys. Med. Biol.* 28 (5) (1983) 565.
- [11] D.A. Jaffray, J.J. Battista, A. Fenster, P. Munro, *Med. Phys.* 22 (7) (1995) 1077.
- [12] GEANT 4 Collaboration, *Physics Reference Manual*, <http://geant4.web.cern.ch/geant4/G4UsersDocuments/UsersGuides/PhysicsReferenceManual>, 2003.
- [13] E. Dermott, TART 2002, A coupled neutron–photon 3-D, combinatorial geometry time dependent Monte Carlo transport code, Cullen University of California, Lawrence Livermore National Laboratory, <http://www.llnl.gov/cullen1>, 2003.
- [14] F. Salvat, J.M. Fernandez-Varea, J. Sempau, PENELOPE, a code system for Monte Carlo simulation of electron and photon transport, Facultat de Física (ECM), Universitat de Barcelona, Spain, 2003.
- [15] I. Kawrakow, D.W.O. Rogers, The EGSnrc code system: Monte Carlo simulation of electron and photon Transport, NRCC Report PIRS-701, <http://www.irs.inms.nrc.ca/inms/irs/EGSnrc/EGSnrc.html> 2003.
- [16] H.P. Chan, K. Doi, *Med. Phys.* 12 (2) (1985) 153.
- [17] J.H. Hubbel, S.M. Seltzer, *Tables of X-ray mass attenuation coefficients and mass energy absorption coefficients 1 keV to 20 MeV for elements Z = 1 to 92 and 48 additional substances of dosimetric interest*. US Department of Commerce, NISTIR 5632, 1995.
- [18] <ftp://physics.nist.gov/PhysRefData/>
- [19] [ftp://www-physics.llnl.gov/pub/rayleigh/RTAB/data\\_NF/](ftp://www-physics.llnl.gov/pub/rayleigh/RTAB/data_NF/)
- [20] J.M. Boone, X-ray production, interaction, and detection in diagnostic imaging, in: J. Beutel, H.L. Kundel, R.L. Van Metter (Eds.), *Physics and Psychophysics, Handbook of Medical Imaging*, vol. 1, SPIE Press, Bellingham, 2000, p. 40.
- [21] H.P. Chan, K. Doi, *Med. Phys.* 11 (4) (1984) 480.
- [22] H.P. Chan, K. Doi, *Med. Phys.* 13 (8) (1986) 824.
- [23] G. Blasse, B.C. Grabmaier, *Luminescent Materials*, Springer, Berlin, Heidelberg, 1994, p. 85.
- [24] G. Blasse, *J. Lumin.* 60–61 (1994) 930.
- [25] T. Kano, *Principal phosphor materials and their optical properties*, in: S. Shionoya, W.M. Yen (Eds.), *Phosphor Handbook*, CRC Press, Boca Raton, FL, 1999, pp. 177–186.
- [26] H. Wiczorek, *Radiat. Meas.* 33 (2001) 541.
- [27] J.A. Rowlands, Flat Panel Detectors for Digital Radiography, in: J. Beutel, H.L. Kundel, R.L. Van Metter (Eds.), *Handbook of Medical Imaging*, Vol. 1, Physics and Psychophysics, SPIE Press, Bellingham, 2000, pp. 234–248.
- [28] A. Baciero, L. Placentino, K.J. McCarthy, L.R. Barquero, A. Ibarra, B. Zurro, *J. Appl. Phys.* 85 (9) (1999) 6790.
- [29] I. Kandarakis, D. Cavouras, E. Ventouras, C. Nonicos. *Radiat. Phys. Chem.* 66 (2003) 257.
- [30] H.W. Vanema, *Radiology* 130 (1979) 765.
- [31] J.H. Hubbel, P.N. Trehan, N. Singh, B. Chand, D. Mehta, M.L. Garg, R.R. Garg, S. Singh, S. Puri, *J. Phys. Chem. Ref. Data.* 23 (2) (1994) 339.
- [32] J.M. Bonne, V.N. Cooper, *Med. Phys.* 27 (6) (2000) 1294.